Applied Catalysis B: Environmental 162 (2015) 372–380

Contents lists available at ScienceDirect

Applied Catalysis B: Environmental

journal homepage: www.elsevier.com/locate/apcatb

# Ni@Pd core–shell nanoparticles modified fibrous silica nanospheres as highly efficient and recoverable catalyst for reduction of 4-nitrophenol and hydrodechlorination of 4-chlorophenol

Zhengping Dong*, Xuanduong Le, Chunxu Dong, Wei Zhang, Xinlin Li, Jiantai Ma*

*College of Chemistry and Chemical Engineering, Gansu Provincial Engineering Laboratory for Chemical Catalysis, Lanzhou University, Lanzhou 730000, PR China*

ARTICLE INFO

*Article history:*
Received 21 April 2014
Received in revised form 8 June 2014
Accepted 3 July 2014
Available online 11 July 2014

*Keywords:*
Ni@Pd/KCC-1 nanocatalyst
Reduction
Hydrodechlorination
4-Nitrophenol
4-Chlorophenol

ABSTRACT

In this study, a novel fibrous nano-silica (KCC-1) based nanocatalyst (Ni@Pd/KCC-1) was synthesized by modifying KCC-1 using Ni@Pd core–shell nanoparticles (NPs). The Ni@Pd/KCC-1 was used in the catalytic reduction of 4-nitrophenol (4-NP) and hydrodechlorination (HDC) of 4-chlorophenol (4-CP). KCC-1, prepared by hydrothermal method, exhibited a dandelion-like shape, high surface area, and easy accessibility of active sites. The Ni@Pd NPs possessed a magnetic nickel (Ni) core with palladium (Pd) shell structural composite. Thus, use of Ni led to the reduced consumption of Pd without sacrificing the overall catalytic performance, simultaneously making it reusable as it could be conveniently recovered from the reaction mixture by using an external magnetic field. Immobilization of the Ni@Pd NPs on KCC-1 nanospheres not only prevented their aggregation, but also significantly enhanced the accessibility of the catalytic active sites. The Ni@Pd/KCC-1 nanocatalyst displayed excellent catalytic activities for both the reduction of 4-NP and the HDC of 4-CP under green conditions. The above-mentioned approach based on fibrous KCC-1 and Ni@Pd NPs provided a useful platform for the fabrication of noble metal-based cost-effective nanocatalyst with easy accessibility, and acted as a promising candidate for numerous catalytic applications.



## 1. Introduction

Nitrophenols (NP) are among the most refractory water pollutants with carcinogenic character and high toxicity. In particular, 4-nitrophenol (4-NP) is a notorious industrial pollutant and environmentally hazardous material exhibiting high solubility and stability in water. 4-NP polluted water poses significant environmental and public health hazards [1–4]. Moreover, chlorophenols (CP), extensively employed in the manufacture of pesticides, disinfectants, and wood preservatives, are toxic, biorefractory, and bioaccumulative [5–8]. Therefore, the United States Environmental Protection Agency has listed most of the NP and CP as priority pollutants. Currently, many processes are developed for the disposal of these pollutants [9–12]. Among the processes contributing to the remediation of 4-NP, reduction of the nitro group is certainly the most characteristic one. Moreover, the reduction product 4-aminophenol (4-AP) is an extremely useful organic compound employed in various applications [13]. Hydrodechlorination (HDC) is considered as the most effective method for the disposal of CP, because the only product (phenol) can be subsequently recycled [14,15]. Till today, it is still necessary to develop low-cost, effective catalysts for the reduction of NP and HDC of CP from concentrated industrial effluents.

Recently, noble metal nanoparticles (NPs), in particular, palladium (Pd) NPs, have been extensively studied as catalysts due to their high catalytic activity for many organic catalytic reactions [16–20]. The catalytic activity of noble metal NPs is mainly dependent on their size, shape, crystallinity, and the surface state. Moreover, the development of nano-sized metal catalysts on catalyst supports has attracted considerable attention. Various supporting materials have been utilized to load Pd NPs as catalysts for organic catalytic reactions, including $Pd/Al_2O_3$ [21], $Au@Pd@TiO_2$ [22], Pd/SBA-15 [23] and Pd/C nanospheres [24]. All the above-mentioned materials have large specific surface areas and pores leading to the homogeneous dispersion of the catalytic sites, thus preventing the aggregation of NPs and improving the catalytic activity of the system. However, poor accessibility to these active sites inside the pores limits their applications for which

* Corresponding authors. Tel.: +86 0931 8912577; fax: +86 0931 8912582.
*E-mail addresses:* dongzhp@lzu.edu.cn (Z. Dong), majiantai@lzu.edu.cn (J. Ma).

http://dx.doi.org/10.1016/j.apcatb.2014.07.009
0926-3373/

significant mass transport is essential. Therefore, silica supports with easily accessible high surface areas, not due to the pores, are highly desirable.

Noticeably, most noble metal NPs catalytic reactions occur only on the surface of the NPs and a large fraction of atoms in the core are catalytically inactive. Therefore, to make a large percentage of noble metal atoms available for catalysis and to reduce their consumption, the inner noble metal atoms should be replaced by other non-noble metals. The presence of a different metal core usually provides control over the catalytic activity, selectivity, and stability owing to "synergistic effects" arising from core–shell metal interaction [25]. Among various non-noble metals, transition Fe-group metals such as Fe, Co, and Ni are often hybridized with noble metals to form magnetic NPs that can be conveniently recovered by using an external magnetic field [26–28]. However, cost-effective noble metal NPs catalysts with inactive cores, excellent catalytic activities, and efficient recoverable properties are extremely rare.

Therefore, in this study, we envisioned that the preparation of Ni@Pd magnetic core–shell NPs could reduce the consumption of Pd. And the immobilization of Ni@Pd NPs on the fibrous silica nanospheres (KCC-1) to fabricate the nanocatalyst Ni@Pd/KCC-1 would be promising for the purpose of preventing the aggregation of Ni@Pd NPs, increasing the accessibility of the active sites and conferring magnetic separation property to the nanocatalyst. KCC-1, first reported by Polshettiwar has the easily accessible high surface area attributed to its fibers and not pores [29,30]. In our previous work, we synthesized Ag/KCC-1 nanocatalyst with easy accessibility and excellent catalytic activity for the reduction of 4-NP and 2-nitroaniline (2-NA) using sodium borohydride ($NaBH_4$) in water at room temperature [31]. Here, the Ni@Pd/KCC-1 nanocatalyst was employed as highly efficient catalyst for the reduction of 4-NP and HDC of 4-chlorophenol (4-CP) under eco-friendly conditions. Importantly, the Ni cores of the Ni@Pd NPs reduced the consumption of Pd, simultaneously making the catalyst reusable due to its convenient recovery. Immobilization of the noble metal NPs with magnetic cores on the supports with high accessibility is a novel method to prepare catalysts with excellent catalytic activities and easily recovered properties; thus, exhibiting potential applications in numerous noble metals NPs based catalytic applications.

## 2. Experimental

### 2.1. Materials

Nickel(II) acetate tetrahydrate ($Ni(ac)_2{\cdot}4H_2O$), palladium(II) bromide ($PdBr_2$), oleyl amine (OAm), trioctylphosphine (TOP), chromatographically pure ethyl acetate ($CH_3COOC_2H_5$) and 3-mercaptopropyltriethoxysilane (MPTES) were purchased from Sigma–Aldrich and used as received. All other chemicals were of the reagent-grade purchased from Tianjing Guangfu Chemical Company and used as supplied. All solvents used for synthesis and measurements were redistilled before use.

### 2.2. Synthesis of Ni@Pd NPs

Ni@Pd core–shell NPs were synthesized via a one-pot high-temperature solution phase synthesis including the consecutive reduction of nickel (II) and palladium (II) in OAm as reported by Sun et al. [25]. Detailed synthetic procedures of the Ni@Pd NPs were shown in the supporting information.

### 2.3. Preparation of KCC-1

In this study, KCC-1 was successfully synthesized by a hydrothermal method instead of the reported microwave assisted technique [31]. The detailed experimental procedure was similar to the microwave assisted hydrothermal method and can be seen in the supporting information.

### 2.4. Fabrication of Ni@Pd/KCC-1

The schematic describing the preparation of Ni@Pd/KCC-1 is shown in Scheme 1. Firstly, 1 g of KCC-1 was added to 100 mL of anhydrous toluene under ultrasonic treatment for 10 min to disperse it homogeneously. Secondly, 0.3 g of MPTES was added dropwise, and the mixture was refluxed for 10 h in a $N_2$ atmosphere. Thirdly, the mixture was cooled to room temperature and the resulting mercaptopropyl functionalized KCC-1 (HS-KCC-1) was centrifuged; washed repeatedly with chloroform, dichloromethane, and ethanol; and finally dried in vacuum. Finally, 0.40 g of HS-KCC-1 was ultrasonically dispersed in 50 mL $H_2O$, and 0.08 g of Ni@Pd NPs was added. After being stirred and ultrasonically dispersed for 1 h, Ni@Pd/KCC-1 was obtained by centrifugation and dried in a vacuum.

### 2.5. Characterization

The size and morphology of the samples and the energy dispersive spectrometer (EDS) were observed by a Tecnai $G^2$ $F^{30}$ transmission electron microscopy (TEM) and samples were obtained by placing a drop of a colloidal solution onto a copper grid and evaporating the solvent in air at room temperature. XRD measurements were performed on a Rigaku D/max-2400 diffractometer using Cu-K$\alpha$ radiation as the X-ray source in the $2\theta$ range of 10–80°. Magnetic measurements of Ni@Pd NPs and Ni@Pd/KCC-1 nanocatalyst were investigated with a quantum design vibrating sample magnetometer (VSM) at room temperature in an applied magnetic field sweeping from −15 to 15 kOe. X-ray photoelectron spectroscopy (XPS) was recorded on a PHI-5702, and the C1S line at 291.4 eV was used as the binding energy reference. The nitrogen adsorption/desorption experiments were performed at 77 K in a micromeritics ASAP 2010 (USA). Elemental analysis (GmbH Vario El Elementar) and inductively coupled plasma atomic emission spectroscopy (ICP-AES) were employed to measure the N, C, H and Ni, Pd content of the samples. Thermal gravimetric analysis (TGA, Perkin Elmer Thermal Analyzer) and Fourier transform infrared spectrometer (FTIR, Bruker IFS66/S) were also used to characterize the samples KCC-1 and Ni@Pd/KCC-1. Ultraviolet–visible (UV–vis) absorption spectra were recorded with a TU-1901 UV-Vis spectrophotometer. The reaction conversion of the HDC reaction was estimated by using GC–MS (Shimazu QP2010S).

### 2.6. General procedure for the reduction of 4-nitrophenol

Firstly, 2.5 mL of aqueous 4-NP solution (0.12 mM) was mixed with 0.5 mL of freshly prepared aqueous $NaBH_4$ solution (0.5 M) and a deep yellow solution was formed. Then, 40 μL of catalyst (concentration 10 mg/mL) was added to the above yellow solution and the reaction was finished until the solution became colorless. The reaction progress was monitored by measuring the UV–vis absorption spectra of the reaction mixture.

The reduction reaction was amplified 20 times to study the reusability of the prepared catalyst. The catalyst was recovered by using a magnet and then washed with water and dried in vacuo at room temperature for the next catalytic run. This procedure was repeated six times.

### 2.7. General procedure for the HDC of 4-chlorophenol

The batch experiments for 4-CP HDC were performed in a 100 mL three-necked flask [14,32]. To evaluate the catalyst activity under green conditions, reaction conditions were established at

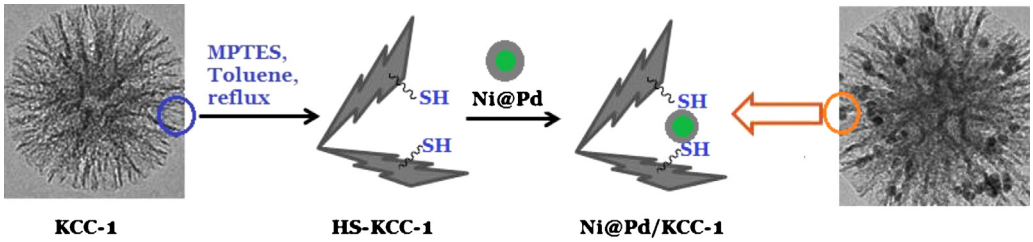


**Scheme 1.** Preparation of Ni@Pd/KCC-1 nanocatalyst.

20 °C and atmospheric pressure, the $H_2$ flow rate of 60 mL/min and a stirring speed of 600 rpm were set. Typically, 10 mg of catalyst, 165 mg of NaOH were suspended in 50 mL deionized water, then 513 mg of 4-CP was added to the solution followed by bubbling $H_2$ and the reaction was timed immediately. To evaluate the conversion of the reaction, the sample was collected with a glass syringe at an interval of 5 min, and then passed through a 0.45 μm membrane filter. The filtrate was extracted by chromatographically pure $CH_3COOC_2H_5$, then the reaction conversion of the HDC reaction was estimated by using GC–MS.

The catalyst used in the HDC reaction was recovered by using a magnet and then washed with water and dried in vacuo at room temperature for the subsequent catalytic run. And the catalytic procedure was repeated six times.

## 3. Results and discussion

### 3.1. Catalysts characterization

In this study, Ni@Pd NPs were prepared by the reduction of $PdBr_2$ on the surface of Ni NPs. OAm was used as a solvent, surfactant, and reductant in the presence of a trace amount of TOP. As reported by Sun et al., the Ni–TOP complex decomposed at 190 °C, while the Pd–TOP complex decomposed above 200 °C, therefore, the Ni core was generated first, followed by the formation of Pd shell [25]. Fig. 1a exhibits the TEM image of the as-prepared Ni@Pd NPs with a uniform spherical shape, resulting from a minimized surface energy [33]. The Ni@Pd NPs have a narrow size distribution with a mean particle size of about 10.2 nm (Fig. 1a, inset).

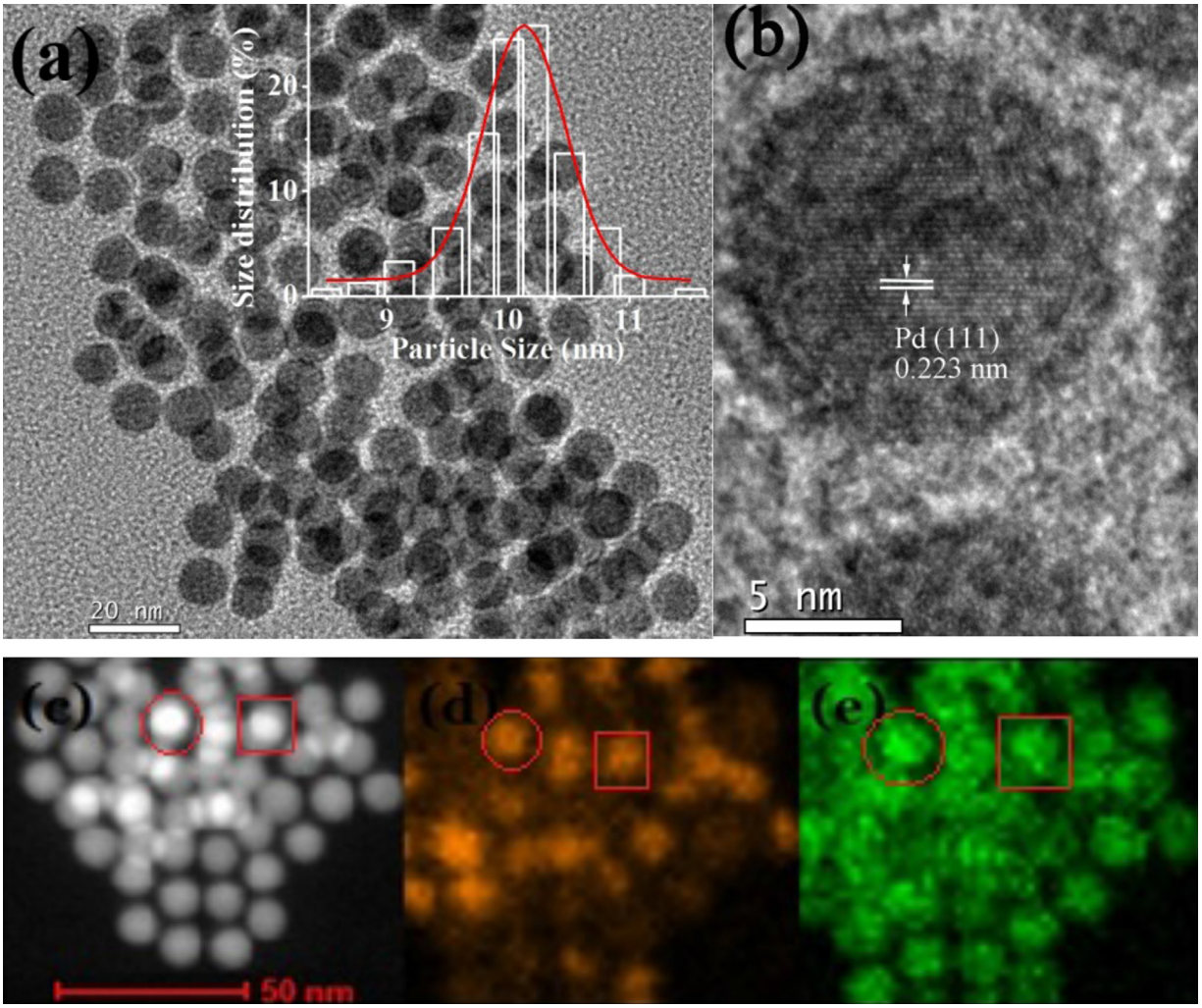


**Fig. 1.** (a) TEM image, (b) HRTEM image, (c) the HAADF-STEM image, (d) the corresponding high resolution Ni mapping and (e) the corresponding high resolution Pd mapping of Ni@Pd NPs. (For interpretation of the references to color in the text citation of this figure, the reader is referred to the web version of this article.)

Moreover, the TEM image reveals the aggregation of a large number of Ni@Pd NPs with each other. High resolution transmission electron microscopy (HRTEM) image (Fig. 1b) shows the polycrystalline structure of the Ni@Pd NPs. Some of the lattice fringes have a distance of 0.223 nm, which is close to the lattice spacing of the (1 1 1) planes of the face-centered cubic (fcc) Pd crystal. Moreover, a high-angle annular dark-field scanning transmission electron microscopy (HAADF-STEM) image (Fig. 1c) was obtained to confirm the core–shell structure of Ni@Pd NPs. The selected-area element analysis greyscale mapping of Ni (Fig. 1d) and Pd (Fig. 1e) clearly defines the core–shell structure with Ni atoms centered in the core (red) and Pd atoms (green) surrounding the Ni core.

The objective of this study was to immobilize the Ni@Pd NPs on KCC-1 to overcome the problem of aggregation of the Ni@Pd NPs and enhance its catalytic activity [29]. Initially, the KCC-1 was functionalized using MPTES. The mercaptopropyl groups acted as robust anchors for the immobilization of Ni@Pd NPs. This process can also prevent the leaching of Ni@Pd NPs from their support (Scheme 1). Fig. 2a illustrates the morphology of KCC-1 demonstrating its porous fibrous structure and uniform spherical shape, with diameters between 200 and 300 nm. The HRTEM image shown in Fig. 2b further elucidates that the distance between the two fibers is around 20 nm (Fig. 2b). The large distance between fibers and the high surface area of KCC-1 (Table S1) leads to the easy loading of Ni@Pd NPs with diameters about 10 nm onto KCC-1 nano-silica. It also prevents the aggregation of the Ni@Pd NPs and increases the accessibility of the active site of the Ni@Pd/KCC-1 nanocatalyst. TEM images of the Ni@Pd/KCC-1 sample are shown in Fig. 2c and

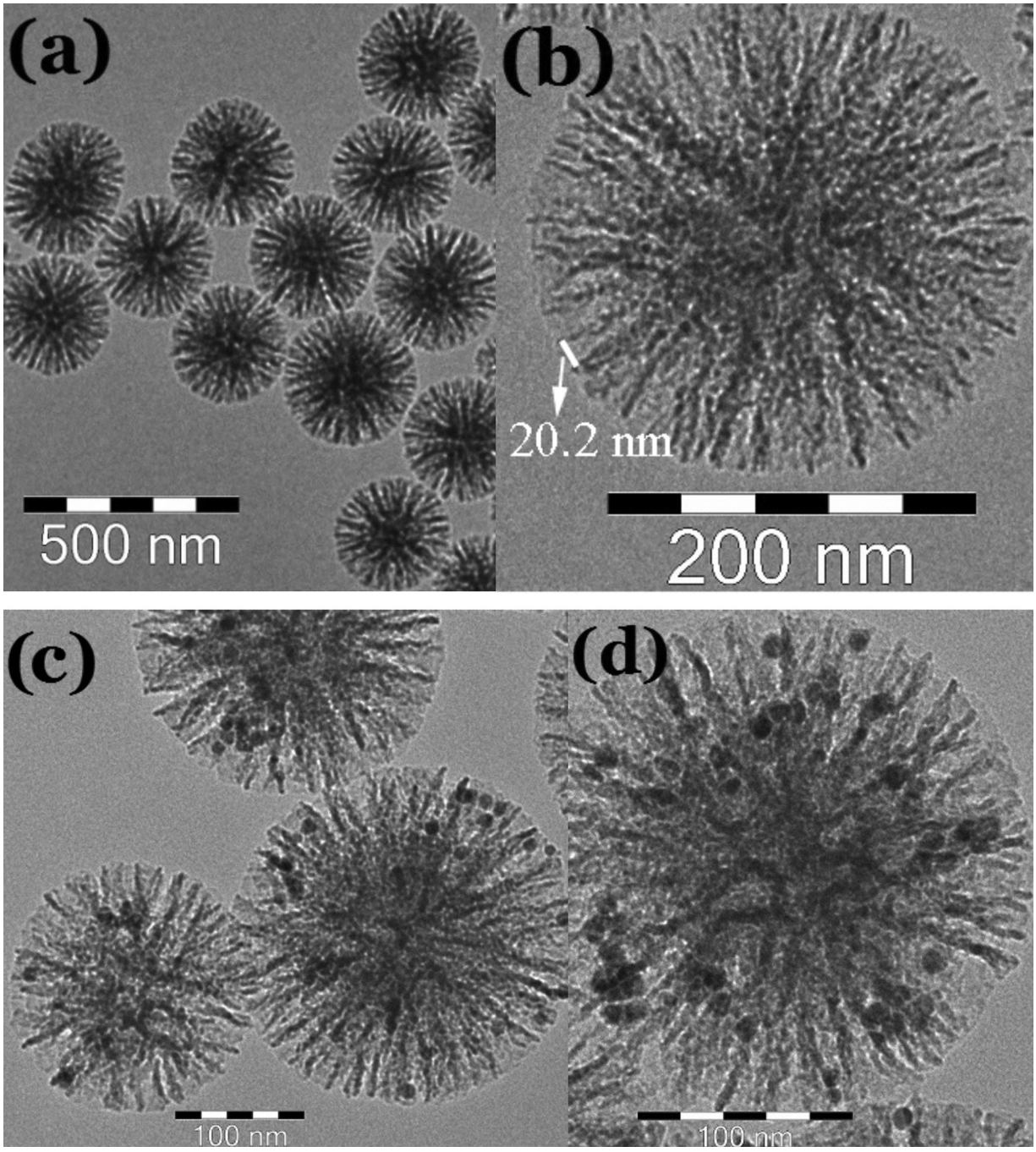


**Fig. 2.** (a) TEM and (b) HRTEM image of KCC-1; (c) TEM and (d) HRTEM image of Ni@Pd/KCC-1 nanocatalyst.

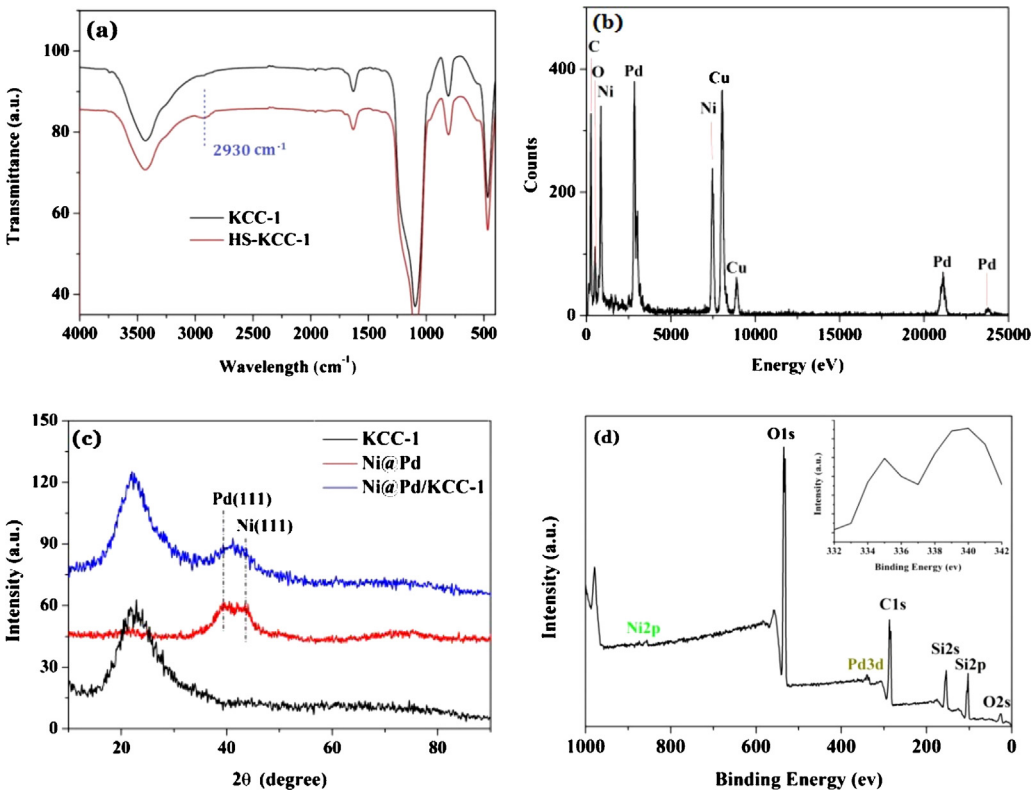


**Fig. 3.** (a) FTIR spectra of KCC-1 and HS-KCC-1, (b) EDS spectra of Ni@Pd NPs, (c) XRD pattern of KCC-1, Ni@Pd NPs and Ni@Pd/KCC-1 nanocatalyst, (d) XPS wide-scan spectrum of the Ni@Pd/KCC-1 nanocatalyst (inset is the XPS spectrum of the spent Pd(0) catalyst).

d. The Ni@Pd NPs are remarkably modified between the fibers of the KCC-1 microspheres, and no obvious aggregation is observed. ICP-AES analysis revealed that the content of Ni@Pd NPs loaded on the surface of KCC-1 was about 16.6% (Table S1).

The FTIR spectra of KCC-1 and HS-KCC-1 are shown in Fig. 3a. In the two samples, the typical Si–O–Si bands around 1100 and 800 $cm^{-1}$ associated with the formation of a condensed silica network. Compared with the spectrum of KCC-1, the FTIR band observed at 2930 $cm^{-1}$ for HS-KCC-1 could be attributed to the C—H stretching frequency. So, it is obvious that the mercaptopropyl groups were efficiently grafted onto the fibers of KCC-1. The TGA curves of KCC-1 and HS-KCC-1 were measured in Ar atmosphere to examine the content of the mercaptopropyl groups loaded on HS-KCC-1. From the weight loss results, it can be seen that the amount of mercaptopropyl groups grafted to the KCC-1 is about 4.5 wt%, which is about the same with the results calculated from the elemental analysis (Fig. S1; Table S1). The EDS analysis was utilized to determine the chemical composition of Ni@Pd NPs. Fig. 3b exhibits the peaks corresponding to Ni and Pd indicating the compositions of Ni@Pd NPs. The peak of copper (Cu) arises from Cu grid in TEM analysis. Moreover, XRD analysis provided evidence for the composition of Ni@Pd NPs and Ni@Pd/KCC-1 nanocatalyst. As shown in Fig. 3c, the wide hump in the range of 2$\theta$ from 15 to 30° was characteristic of the amorphous silica of KCC-1. However, the XRD pattern of Ni@Pd NPs shows the broad peaks representing the Pd (1 1 1) and Ni (1 1 1). The XRD pattern of Ni@Pd/KCC-1 nanocatalyst obtained after the modification of Ni@Pd NPs on KCC-1, revealed the presence of all the expected characteristic peaks of Ni@Pd NPs along with the peak corresponding to amorphous silica, indicating the successful immobilization of Ni@Pd NPs on KCC-1. Fig. 3d displays the XPS analysis to examine the valence states of Pd on the surface of Ni@Pd NPs. The XPS elemental survey scan of the surface of Ni@Pd/KCC-1 nanocatalyst microspheres revealed the presence of silicon, oxygen, Ni, Pd, and carbon elements in the samples. As shown in Fig. 3d, inset, the peaks observed in the XPS spectra of Pd 3d at binding energies of 335.1 and 340.2 eV are characteristic of metallic Pd.

Magnetization curves (Fig. 4) show the superparamagnetic behavior of the Ni@Pd NPs and Ni@Pd/KCC-1 nanocatalyst. The magnetic saturation values of the Ni@Pd NPs and Ni@Pd/KCC-1 nanocatalyst are 4.63 and 0.78 emu $g^{-1}$, respectively. Therefore, the Ni@Pd NPs modified Ni@Pd/KCC-1 nanocatalyst could be efficiently separated from the solution by using an external magnetic force and could be reused and recycled (Fig. 4 inset).

### 3.2. Catalytic reduction of 4-NP

The catalytic activity of the Ni@Pd/KCC-1 nanocatalyst was established by the reduction of 4-NP to 4-AP in the presence of $NaBH_4$ (Scheme 2). The evolution process with reaction time for

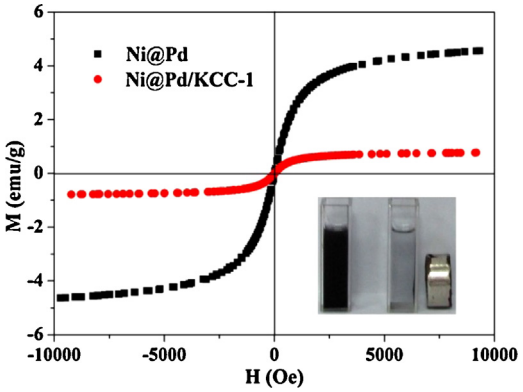


**Fig. 4.** Room temperature magnetization curves of Ni@Pd NPs and Ni@Pd/KCC-1 nanocatalyst.

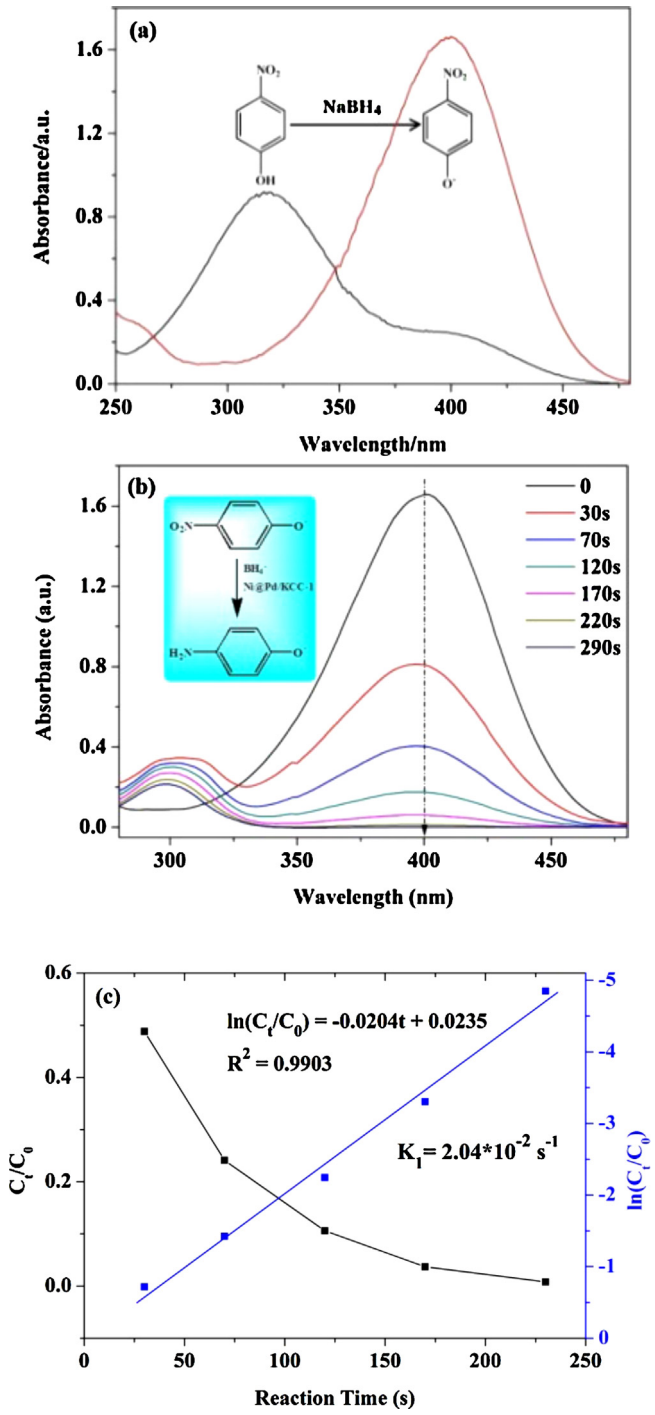


**Fig. 5.** UV–vis spectra of 4-NP before and after adding $NaBH_4$ solution (a), the successive reduction of 4-NP to 4-AP over the prepared Ni@Pd/KCC-1 nanocatalyst (b), and plots of $C_t/C_0$ and $\ln(C_t/C_0)$ versus reaction time for the reduction of 4-NP over Ni@Pd/KCC-1 nanocatalyst (c).

the reduction of 4-NP to 4-AP was monitored by UV–vis spectroscopy. Solution of 4-NP exhibits a strong absorption peak at 317 nm which is remarkably red-shifted to 400 nm when treated with an aqueous solution of $NaBH_4$, due to the formation of 4-nitrophenolate ions (Fig. 5a) [34–42]. This process accompanies a color change from pale yellow to bright yellow (Fig. S2). Moreover, the maximum absorption did not change over time, even after adding superfluous $NaBH_4$ solution, confirming that the reduction did not proceed by aqueous $NaBH_4$ solution. The addition of Ni@Pd/KCC-1 nanocatalyst (0.4 mg) into the system led to the decrease in the peak intensity of 4-nitrophenolateion at 400 nm with the concomitant increase in the peaks corresponding to 4-AP at 300 nm. The reaction proceeds rapidly with the conversion exceeding 99.8% at a reaction time of about 4 min (Fig. 5b). After the completion of the reaction, the reaction mixture became colorless (Fig. S2).

The reaction conversion is calculated from $C_t/C_0$ (Fig. 5c), measured by using the relative intensity of UV–vis absorbance ($A_t/A_0$) at 400 nm. Herein, $C_t$ is the concentration of 4-NP at the reaction time $t$ and $C_0$ is the initial concentration. The concentration of $NaBH_4$ was much higher than that of 4-NP and thus considered as constant during the course of the reaction. Therefore, the reduction reactions were assumed to be pseudo first-order with respect to the concentration of 4-NP [22,43]. As shown in Fig. 5c, the plots $\ln(C_t/C_0)$ versus reaction time shows a straight line, indicating the appropriate coincidence with the pseudo first-order equation. Therefore, the reaction kinetic can be described as $\ln(C_t/C_0) = -kt$, where $k$ is the apparent first-order rate constant ($s^{-1}$), and $t$ is the reaction time (s). The reaction rate constant $k$ was calculated to be $2.04 \times 10^{-2}$ $s^{-1}$ for the reaction catalyzed using Ni@Pd/KCC-1 nanocatalyst. The results of ICP-AES analysis (Table S1) revealed that the Pd active sites added to the reaction were about 0.04 mg. Thus, for a quantitative comparison, the activity parameter $k_{Pd} = k/M$ was introduced, which is defined as the ratio of the rate constant $k$ to the weight of the active sites of Pd added ($M$) [34,44]. The reaction rate constant per unit mass ($M_{Pd}$) was calculated to be $k_{Pd} = 510\ s^{-1}\ g^{-1}$ by using the above-mentioned condition, for the reduction of 4-NP using Ni@Pd/KCC-1 nanocatalyst.

Moreover, the unsupported Ni@Pd NPs were also used as catalyst for the reduction of 4-NP and the results are displayed in Fig. 6. The amount of the Ni@Pd NPs used in the reduction reaction was 0.067 mg, which contained about 0.04 mg Pd, thus the amount of the Pd active sites was similar to that in the Ni@Pd/KCC-1 nanocatalyst. Fig. 6a demonstrates that the reduction reaction was much faster in the very beginning. However, the reaction rate decreased gradually with the reaction time. In Fig. 6b, the kinetics of the reduction of 4-NP did not show a straight line. It is worth mentioning that the reaction kinetics could be divided into two parts: before 200 s, the reaction kinetics was almost a straight line, and the reaction rate constant $k_1$ was calculated to be $1.3 \times 10^{-2}\ s^{-1}$ ($k_{1Pd} = 325\ s^{-1}\ g^{-1}$). From 200 s to 303 s, the reaction kinetics showed a straight line and $k_2$ was calculated to be $1.5 \times 10^{-3}\ s^{-1}$ ($k_{2Pd} = 37.5\ s^{-1}\ g^{-1}$). The above-mentioned phenomena may be due to two reasons: first, the gradual aggregation of the Ni@Pd NPs with the progress of the reaction, leading to the reduction in the reaction rate and reaction rate constant. Second, the catalyst without support has poor mass transfer. In the process of catalytic reaction, products block the clearance between NPs; therefore, the reactants cannot contact the catalyst, resulting in decreased reaction rate [45]. The comparison between the Ni@Pd/KCC-1 nanocatalyst and Ni@Pd NPs obviously showed that Ni@Pd/KCC-1 nanocatalyst with easy accessibility of the active sites exhibited higher catalytic activity than the unsupported Ni@Pd NPs.

In addition, the catalytic activities of Ni@Pd/KCC-1 nanocatalyst were also compared with other reported noble metal NPs. Zhang et al. [46] reported Pd NPs supported on cellulose nanocrystal with the reduction rate constant of $5.7 \times 10^{-3}\ s^{-1}$. Fang and Wang [47] used sponge-like carbonaceous support to encapsulate Pd NPs, obtaining excellent catalytic performance of Pd/C toward the reduction of nitro-compound with the apparent rate constant of $8.83 \times 10^{-3}\ s^{-1}$. It is therefore concluded that the Ni@Pd/KCC-1 nanocatalyst shows good catalytic activity for 4-NP reduction ($2.04 \times 10^{-2}\ s^{-1}$), which mainly attributes to the clearance between silica fibers of KCC-1 that leads to easy accessibility of the active sites and more efficient mass transport process.

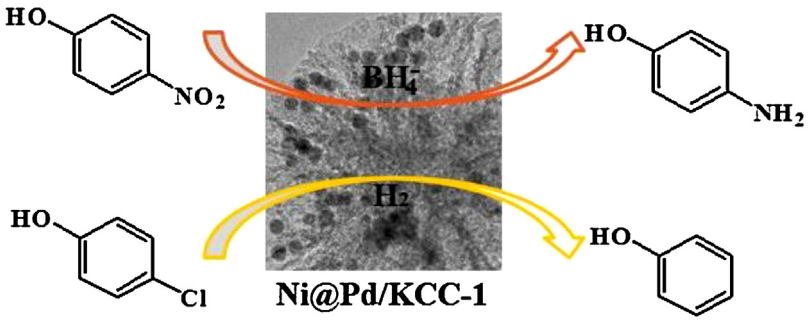


**Scheme 2.** Reduction of 4-NP and HDC of 4-CP, respectively on the surface of Ni@Pd/KCC-1 nanocatalyst.

### 3.3. HDC of 4-CP

In recent years, the catalytic HDC of chlorinated compounds has been a field of remarkable interest because the catalytic treatment is a viable, low-cost, and environmentally friendly approach. Noble metal NPs have been found to be highly active for HDC of 4-CP [32,48–51]. Based on the aforementioned results, the Ni@Pd/KCC-1 nanocatalyst was also used to perform the catalytic HDC of 4-CP. The HDC of 4-CP reactions is always conducted under green conditions. To optimize the reaction conditions, a series of reactions were performed using several bases, solvents, and hydrogen sources to obtain the best possible combination (Figs. S3–S5). The best optimized condition in accordance with the green chemistry was established as follows: water as solvent, sodium hydroxide (NaOH) as a base and $H_2$ as hydrogen source for the catalytic HDC of 4-CP at room temperature [6,52].

Fig. 7a shows the time-dependent concentration of 4-CP and the concentration of the product phenol in the HDC reaction using Ni@Pd/KCC-1 nanocatalyst. The investigation of the reaction conditions revealed the maximum conversion of 4-CP into phenol in 2 h. The GC–MS results indicated that phenol was the only product in the HDC reaction using Ni@Pd/KCC-1 as catalyst, and formation of other species was not observed. Some previous works reported that, the use of Pd based catalysts under mild conditions also generated cyclohexanone as reaction product in addition to phenol [5,53,54]. While the concentration of catalysts and the ratio of catalysts to 4-CP used in those works were much higher than ours. Thus, it is remarkable that, in the operating conditions tested, the lower consumption of Ni@Pd/KCC-1 nanocatalyst used in the current work did not show activity for phenol hydrogenation. Other reported works with lower consumption of catalysts also obtained phenol as the only product [55,56].

The HDC reaction was assumed to be pseudo first-order, because the reducing agent $H_2$ was used excessively compared to 4-CP and could be considered as constant during the course of the reaction [5]. Therefore, by using the reaction kinetics $\ln(C_t/C_0) = -kt$, the reaction rate constant $k$ was calculated to be 0.038 $min^{-1}$ for the reactions catalyzed at room temperature using Ni@Pd/KCC-1 nanocatalyst (Fig. 7b). 4-CP was dechlorinated through hydrogenolysis of C—Cl bond [6]. The reaction pathway is explained as follows: first, $H_2$ was adsorbed on the surface of the Ni@Pd/KCC-1 nanocatalyst and was dissociated into two active hydrogen atoms. Second, the concentration of the 4-CP was extremely high near the surface of Ni@Pd/KCC-1 nanocatalyst owing to the adsorption; therefore, the C—Cl bond of 4-CP was attacked by the active hydrogen atoms to form phenol. Simultaneously, hydrochloric acid (HCl) was produced which reacted rapidly with NaOH present in the reaction system leading to the formation of NaCl that dissolved in water. Thus, the accumulation of HCl on the surface of the catalyst was prevented. Therefore, addition of an excess amount of NaOH against Cl atoms made the reaction system free of the negative effect of HCl and effectively prevented the poisoning of the catalysts [57]. In addition, the HDC of 4-CP was also performed using the Ni@Pd NPs as catalyst (Fig. S6). The amount of the Ni@Pd NPs was similar to that in the Ni@Pd/KCC-1 nanocatalyst. Almost all the 4-CP was converted into phenol in 4 h. Using the reaction kinetics $\ln(C_t/C_0) = -kt$, the reaction rate constant was calculated to be 0.014 $min^{-1}$, which was lower than the Ni@Pd/KCC-1 nanocatalyst (0.038 $min^{-1}$). Thus, the Ni@Pd/KCC-1 nanocatalyst had higher catalytic activities than the unsupported Ni@Pd NPs.

Further, the Ni@Pd/KCC-1 nanocatalyst used for the reduction of 4-NP and HDC of 4-CP in an eco-friendly manner under the green conditions reflects the economic viewpoint. For the reactions using Pd NPs as the catalyst, the catalytic reaction occurs only on its surface and the large fraction of the Pd atoms inside the core are

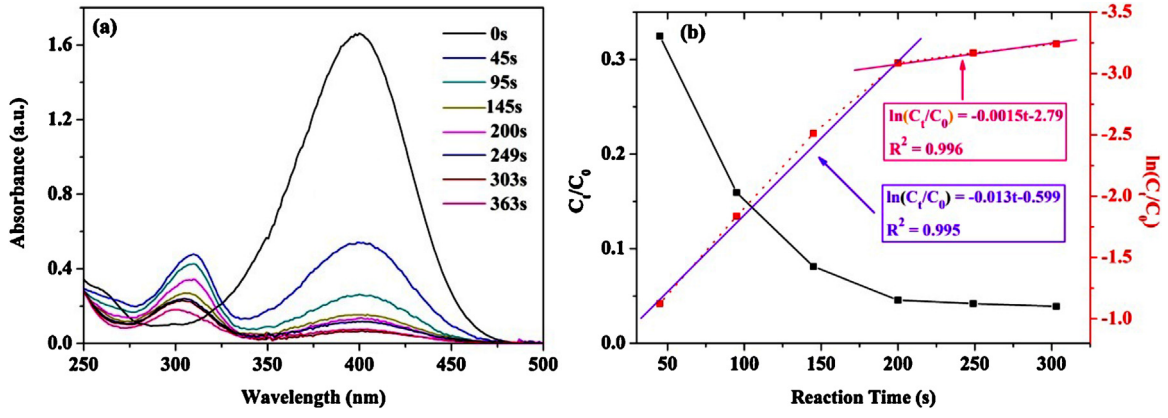


**Fig. 6.** (a) UV–vis spectra of the successive reduction of 4-NP to 4-AP over the prepared Ni@Pd NPs and (b) plots of $C_t/C_0$ and $\ln(C_t/C_0)$ versus reaction time for the reduction of 4-NP over Ni@Pd NPs.

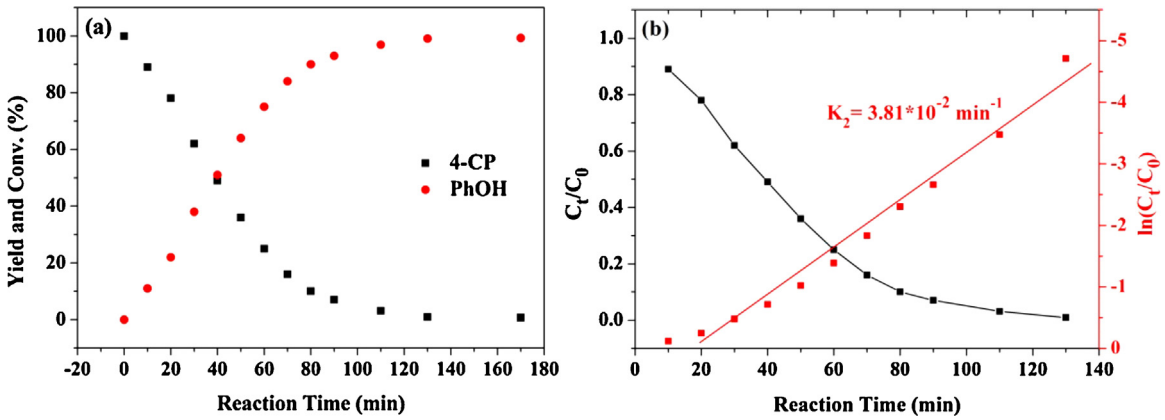


**Fig. 7.** (a) Time evolution of the yield of phenol and conversion of 4-CP with Ni@Pd/KCC-1 catalyst, (b) plots of $C_t/C_0$ and $\ln(C_t/C_0)$ versus reaction time for the HDC of 4-CP over Ni@Pd/KCC-1 nanocatalyst.

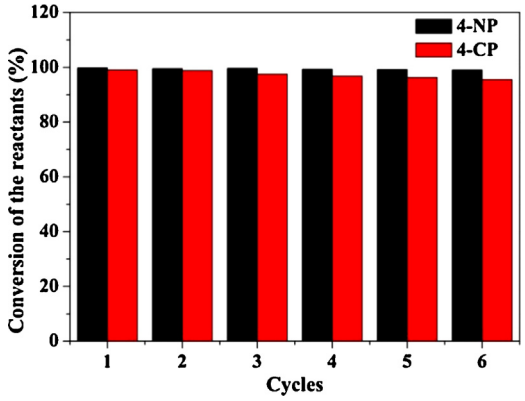


**Fig. 8.** The reusability of Ni@Pd/KCC-1 nanocatalyst for the reduction of 4-NP and HDC of 4-CP.

catalytically inactive. Therefore, the inner Pd atoms are replaced by non-noble Ni atoms, and the Pd atoms as active sites are on the surface of the Ni cores leading to the formation of cost-effective catalyst. Furthermore, magnetic separation is an appealing alternative for filtration or centrifugation as it prevents the loss of catalyst and improves the reusability of the catalyst for liquid-phase reactions [58]. The Ni@Pd NPs based nanocatalyst with magnetic Ni cores were easily recovered from the reaction mixture under an external magnetic field. The recovered Ni@Pd/KCC-1 nanocatalyst was used for at least six runs. There was just a slight trend to deactivation of the Ni@Pd/KCC-1 nanocatalyst in both the reactions as shown in Fig. 8, probably due to the poisoning of the surface Pd catalyst via oxidation or catalyst inactivation. ICP-AES analysis also showed that there was little leaching of the active sites after six catalytic runs (Table S1). The morphology of the Ni@Pd/KCC-1 nanocatalyst used for six cycles was almost maintained (Fig. S7). Thus, the result suggests good stability and reusability of Ni@Pd/KCC-1 nanocatalyst, which mainly attributes to the mercaptopropyl groups on the surface of KCC-1 nanospheres acted as robust anchors to prevent the aggregation and leaching of Ni@Pd NPs from the fibrous support.

## 4. Conclusions

In summary, Ni@Pd core–shell NPs were synthesized via one-pot high temperature solution phase synthesis, including the consecutive reduction of Ni (II) and Pd (II) in OAm. Well defined core–shell structure of Ni@Pd NPs consisted of non-noble metal Ni atoms centered in the core and noble metal Pd atoms surrounding the Ni core. Therefore, the consumption of Pd was reduced without sacrificing the overall catalytic performance. Simultaneously, a large percentage of noble metal atoms were available for catalysis. Thus, expensive Pd metal shell around a cheap Ni metal core led to a cost-effective material for catalysis. When Ni@Pd NPs were immobilized on KCC-1 with easy accessibility of the active sites, the aggregation of Ni@Pd NPs was prevented, and the accessibility of the catalytic active sites was increased significantly. Therefore, Ni@Pd/KCC-1 nanocatalyst showed excellent catalytic activity for the reduction of 4-NP, with the reaction rate constant $k$ of about $2.04 \times 10^{-2}$ s$^{-1}$ and it was also effective for the HDC of 4-CP. Moreover, the Ni@Pd/KCC-1 nanocatalyst could be easily recovered from the reaction mixture by using a magnet and reused for the next catalytic run due to the superparamagnetic behavior of the magnetic Ni core. The Ni@Pd/KCC-1 nanocatalyst was stable and could be recycled for at least six times in the corresponding reactions without reduction in the catalytic activity. The Ni@Pd/KCC-1 nanocatalyst acts as relatively green, economical, and environmental friendly catalyst, and as a promising candidate for various Pd based catalytic applications.

## Acknowledgements

The authors acknowledge financial support from the NSFC (Grant 21301082), the Natural Science Foundation of Gansu (No. 1308RJYA028) and the Fundamental Research Funds for the Central Universities (lzujbky-2013-61).

## Appendix A. Supplementary data

Supplementary data associated with this article can be found, in the online version, at http://dx.doi.org/10.1016/j.apcatb.2014.07.009.

## References

[1] J. Feng, L. Su, Y. Ma, C. Ren, Q. Guo, X. Chen, Chem. Eng. J. 221 (2013) 16–24.
[2] B. Lai, Z. Chen, Y. Zhou, P. Yang, J. Wang, Z. Chen, J. Hazard. Mater. 250 (2013) 220–228.
[3] M. Zarejousheghani, M. Moeder, H. Borsdorf, Anal. Chim. Acta 798 (2013) 48–55.
[4] M.L. Wang, T.T. Jiang, Y. Lu, H.J. Liu, Y. Chen, J. Mater. Chem. A 1 (2013) 5923–5933.
[5] E. Diaz, J.A. Casas, A.F. Mohedano, L. Calvo, M.A. Gilarranz, J.J. Rodriguez, Ind. Eng. Chem. Res. 47 (2008) 3840–3846.
[6] S. Wang, B. Yang, T. Zhang, G. Yu, S. Deng, J. Huang, Ind. Eng. Chem. Res. 49 (2010) 4561–4565.
[7] T. Faludi, N. Andrasi, A. Vasanits-Zsigrai, G. Zaray, I. Molnar-Perl, J. Chromatogr. A 1302 (2013) 133–142.

[8] S. Holopainen, V. Luukkonen, M. Nousiainen, M. Sillanpaa, Talanta 114 (2013) 176–182.
[9] M.-Q. Yang, X. Pan, N. Zhang, Y.-J. Xu, CrystEngComm 15 (2013) 6819–6828.
[10] R. Bhandari, M.R. Knecht, ACS Catal. 1 (2011) 89–98.
[11] Z. Wu, M. Zhang, Z. Zhao, W. Li, K. Tao, J. Catal. 256 (2008) 323–330.
[12] F. Coccia, L. Tonucci, D. Bosco, M. Bressan, N. d'Alessandro, Green Chem. 14 (2012) 1073–1078.
[13] S.M. El-Sheikh, A.A. Ismail, J.F. Al-Sharab, New J. Chem. 37 (2013) 2399–2407.
[14] J. Zhou, Y. Han, W. Wang, Z. Xu, H. Wan, D. Yin, S. Zheng, D. Zhu, Appl. Catal. B: Environ. 134 (2013) 222–230.
[15] S. Gomez-Quero, F. Cardenas-Lizana, M.A. Keane, AIChE J. 56 (2010) 756–767.
[16] M. Garcia-Melchor, M.C. Pacheco, C. Najera, A. Lledos, G. Ujaque, ACS Catal. 2 (2012) 135–144.
[17] A.L. Isfahani, I. Mohammadpoor-Baltork, V. Mirkhani, A.R. Khosropour, M. Moghadam, S. Tangestaninejad, R. Kia, Adv. Synth. Catal. 355 (2013) 957–972.
[18] Y.P. Shang, X.M. Jie, J. Zhou, P. Hu, S.J. Huang, W.P. Su, Angew. Chem. Int. Ed. 52 (2013) 1299–1303.
[19] H. Kamisaki, T. Nanjo, C. Tsukano, Y. Takemoto, Chem. Eur. J. 17 (2011) 626–633.
[20] H. Li, J.J. Cooper-White, Nanoscale 5 (2013) 2915–2920.
[21] M. Cobo, A. Orrego, J.A. Conesa, Appl. Catal. A: Gen. 445 (2012) 83–91.
[22] W. Hu, B. Liu, Q. Wang, Y. Liu, Y. Liu, P. Jing, S. Yu, L. Liu, J. Zhang, Chem. Commun. 49 (2013) 7596–7598.
[23] J.-H. Park, S.-K. Kim, H.S. Kim, Y.J. Cho, J. Park, K.E. Lee, C.W. Yoon, S.W. Nam, S.O. Kang, Chem. Commun. 49 (2013) 10832–10834.
[24] S. Wang, W.C. Li, G.P. Hao, Y. Hao, Q. Sun, X.Q. Zhang, A.H. Lu, J. Am. Chem. Soc. 133 (2011) 15304–15307.
[25] O. Metin, S.F. Ho, C. Alp, H. Can, M.N. Mankin, M.S. Gultekin, M. Chi, S. Sun, Nano Res. 6 (2013) 10–18.
[26] Z. Abdullaeua, E. Omurzak, C. Iwamoto, H.S. Ganapathy, S. Sulaimankulova, L. Chen, T. Mashimo, Carbon 50 (2012) 1776–1785.
[27] M. Li, X. Chen, J. Guan, X. Wang, J. Wang, C.T. Williams, C. Liang, J. Mater. Chem. 22 (2012) 609–616.
[28] Z. Liu, C. Lv, X. Tan, J. Phys. Chem. Solids 74 (2013) 1275–1280.
[29] V. Polshettiwar, D. Cha, X. Zhang, J.M. Basset, Angew. Chem. Int. Ed. 49 (2010) 9652–9656.
[30] A. Fihri, D. Cha, M. Bouhrara, N. Almana, V. Polshettiwar, ChemSusChem 5 (2012) 85–89.
[31] Z. Dong, X. Le, X. Li, W. Zhang, C. Dong, J. Ma, Appl. Catal. B: Environ. 158–159 (2014) 129–135.
[32] Z. Wu, C. Sun, Y. Chai, M. Zhang, RSC Adv. 1 (2011) 1179–1182.
[33] Y. Wu, D. Wang, P. Zhao, Z. Niu, Q. Peng, Y. Li, Inorg. Chem. 50 (2011) 2046–2048.
[34] J. Zhang, G. Chen, M. Chaker, F. Rosei, D. Ma, Appl. Catal. B: Environ. 132 (2013) 107–115.
[35] H. Yamamoto, H. Yano, H. Kouchi, Y. Obora, R. Arakawa, H. Kawasaki, Nanoscale 4 (2012) 4148–4154.
[36] B. Xia, F. He, L. Li, Langmuir 29 (2013) 4901–4907.
[37] Q. Wang, W. Jia, B. Liu, A. Dong, X. Gong, C. Li, P. Jing, Y. Li, G. Xu, J. Zhang, J. Mater. Chem. A 1 (2013) 12732–12741.
[38] H. Li, L. Han, J. Cooper-White, I. Kim, Green Chem. 14 (2012) 586–591.
[39] A. Shivhare, S.J. Ambrose, H. Zhang, R.W. Purves, R.W.J. Scott, Chem. Commun. 49 (2013) 276–278.
[40] J. Zheng, Y. Dong, W. Wang, Y. Ma, J. Hu, X. Chen, X. Chen, Nanoscale 5 (2013) 4894–4901.
[41] L. Zhang, S. Zheng, D.E. Kang, J.Y. Shin, H. Suh, I. Kim, RSC Adv. 3 (2013) 4692–4703.
[42] M.M. Mohamed, M.S. Al-Sharif, Appl. Catal. B: Environ. 142–143 (2013) 432–441.
[43] H. Gu, J. Wang, Y. Ji, Z. Wang, W. Chen, G. Xue, J. Mater. Chem. A 1 (2013) 12471–12477.
[44] B. Baruah, G.J. Gabriel, M.J. Akbashev, M.E. Booher, Langmuir 29 (2013) 4225–4234.
[45] Z.X. Yan, G.Q. He, G.H. Zhang, H. Meng, P.K. Shen, Int. J. Hydrogen Energy 35 (2010) 3263–3269.
[46] X. Wu, C. Lu, W. Zhang, G. Yuan, R. Xiong, X. Zhang, J. Mater. Chem. A 1 (2013) 8645–8652.
[47] Y. Fang, E. Wang, Nanoscale 5 (2013) 1843–1848.
[48] B. Yang, S. Deng, G. Yu, Y. Lu, H. Zhang, J. Xiao, G. Chen, X. Cheng, L. Shi, Chem. Eng. J. 219 (2013) 492–498.
[49] S. Gomez-Quero, F. Cardenas-Lizana, M.A. Keane, Nanotechnology 23 (2012).
[50] S. Gomez-Quero, F. Cardenas-Lizana, M.A. Keane, J. Catal. 303 (2013) 41–49.
[51] S. Gomez-Quero, F. Cardenas-Lizana, M.A. Keane, Chem. Eng. J. 166 (2011) 1044–1051.
[52] Z.M. de Pedro, E. Diaz, A.F. Mohedano, J.A. Casas, J.J. Rodriguez, Appl. Catal. B: Environ. 103 (2011) 128–135.
[53] M. Munoz, Z.M. de Pedro, J.A. Casas, J.J. Rodriguez, Water Res. 47 (2013) 3070–3080.
[54] C.B. Molina, A.H. Pizarro, J.A. Casas, J.J. Rodriguez, Appl. Catal. B: Environ. 148–149 (2014) 330–338.
[55] H. Rong, S. Cai, Z. Niu, Y. Li, ACS Catal. 3 (2013) 1560–1563.
[56] Y. Lan, L. Yang, M. Zhang, W. Zhang, S. Wang, ACS Appl. Mater. Interfaces 2 (2010) 127–133.
[57] C. Sun, Z. Wu, Y. Mao, X. Yin, L. Ma, D. Wang, M. Zhang, Catal. Lett. 141 (2011) 792–798.
[58] F. Zhang, J. Jin, X. Zhong, S. Li, J. Niu, R. Li, J. Ma, Green Chem. 13 (2011) 1238–1243.